Nonlinearity **12** (1999) 247–268. Printed in the UK PII: S0951-7715(99)92601-4

Breakdown in Burgers-type equations with saturating dissipation fluxes

Jonathan Goodman†, Alexander Kurganov‡§ and Philip Rosenau‡

† Courant Institute of Mathematical Sciences, NYU, New York, NY 10012, USA
‡ School of Mathematical Sciences, Tel-Aviv University, Tel-Aviv 69978, Israel
§ Mittag-Leffler Institute, Djursholm S-182 62, Sweden

Received 19 March 1998
Recommended by G Morriss

Abstract. We study the recently proposed convection–diffusion model equation $u_t + f(u)_x = Q(u_x)_x$, with a bounded function $Q(u_x)$. We consider both strictly monotone dissipation fluxes with $Q'(u_x) > 0$, and nonmonotone ones such that $Q(u_x) = \pm\nu u_x/(1 + u_x^2)$, $\nu > 0$. The novel feature of these equations is that large amplitude solutions develop spontaneous discontinuities, while small solutions remain smooth at all times. Indeed, small amplitude kink solutions are smooth, while large amplitude kinks have discontinuities (*subshocks*). It is demonstrated numerically that both continuous and discontinuous travelling waves are strong attractors of a wide classes of initial data. We prove that solutions with a sufficiently large initial data blow up in finite time. It is also shown that if $Q(u_x)$ is monotone and unbounded, then u_x is uniformly bounded for all times. In addition, we present more accurate numerical experiments than previously presented, which demonstrate that solutions to a Cauchy problem with periodic initial data may also break down in a finite time if the initial amplitude is sufficiently large.

AMS classification scheme numbers: 35Kxx, 35Qxx, 65Mxx

1. Introduction

In this work we continue our studies of the recently proposed convection–diffusion models [12, 11],

$$u_t + f(u)_x = Q(u_x)_x, \tag{1.1}$$

with $Q(u_x)$, the dissipation flux function, assumed to be a bounded function. Though the boundedness of the flux function $Q(u_x)$ is a fundamental property of real physical systems, more often that not this feature is lost in the weakly nonlinear, small gradients expansion. We consider both strictly monotone dissipation fluxes such that $Q'(u_x) > 0$ [12], and nonmonotone ones such that $Q(u_x) = \pm\nu u_x/(1 + u_x^2)$, $\nu > 0$ [11]. The nonconvective, purely diffusive variants of equation (1.1) were proposed in earlier works for both monotone [18, 17, 3, 4], and nonmonotone $Q's$ [17, 15]. Interestingly, the nonmonotone case was proposed at about the same time to describe the evolution of systems with a controlled instability, [17], and in the context of image processing [15]. The monotone dissipation flux $Q(u_x)$ to be adopted, was constructed in [17] as a Padé approximant which correctly connects both the infra-red and ultra-violet limits (for more details see [17]). In the nonmonotone case the flux function we assume is not a replica of a particular response; rather it is intended to be a simple caricature of complex scenarios where the medium yields at a critical stress (say, elasto–plastic transition) or

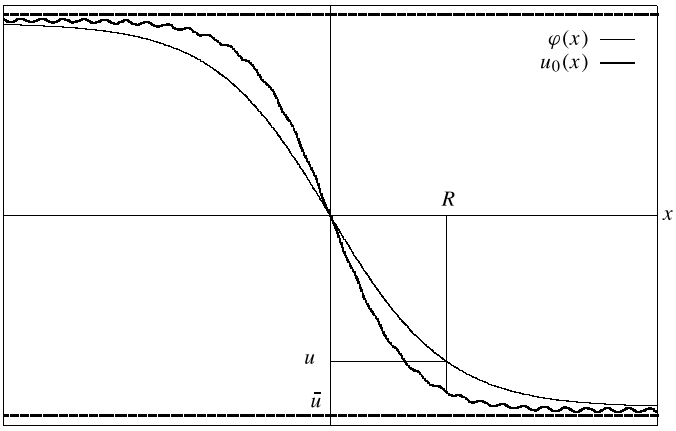

Figure 1. An example of initial data satisfying hypotheses (a)–(d).

undergoes some critical transition. This transition is accompanied by a structural change (say, a non-Newtonian behaviour in complex fluids) and, as a consequence, its dynamical response changes drastically. This critical transition is accompanied by a change of sign of the elliptic part rendering the evolution backward parabolic. However, the saturation of the flux mitigates the instability and instead of a typical amplitude blow up, a much milder effect is observed. For more details see [11].

The novel feature of equations (1.1) as compared with the conventional Burgers equation, is that large amplitude solutions develop discontinuities within finite time, while small solutions remain smooth at all times. This was shown in [12, 11] for the Cauchy problem with sufficiently small, smooth, periodic (or compactly supported) initial data,

$$u(x, t = 0) = u_0(x). \tag{1.2}$$

This feature is best seen in explicit analysis of travelling waves [12, 11]: small amplitude kinks are smooth, while large amplitude kinks have discontinuities (*subshocks*). The resulting subshock jump was calculated and it was demonstrated numerically, that both the continuous and the discontinuous travelling waves are strong attractors of a wide classes of initial data.

In this paper, *we prove that solutions with a certain large initial data blow up in a finite time*. The proof relies on considering the total mass in a box of length R, as in figure 1, and is not an extension of the conventional blowup arguments for Burgers' equation. In addition, we present new, and more accurate numerical experiments then previously presented, which demonstrate that solutions to a Cauchy problem with periodic initial data may also break down within a finite time if the initial amplitude is sufficiently large. The issue of breakdown was left unresolved in [12].

It is useful to provide an intuitive explanation of the dynamics. The critical threshold for a break-up is caused by the imbalance between the convective and dissipative fluxes at high amplitudes. While in the original Burgers model these mechanisms can always balance each other, and as we shall see shortly, this is also true for any Q that is unbounded and increasingly monotone, this changes once the dissipative flux is forced to remain bounded. While the inertial flux can be made arbitrarily large, the dissipative flux responds up to a certain critical amplitude only. At higher amplitudes the mismatch between these two fluxes is resolved by a discontinuous jump(s). Indeed, the interest to capture this kind of behaviour, encountered, for instance, in elasto–plastic transitions, was the main motivation to propose these models [17, 12, 11].

In section 2.1 we consider equation (1.1) with a bounded dissipation flux Q, that increases monotonously and is appended with a smooth, bounded, and infinitely supported initial data, (1.2). In theorem 2.1 we prove that if the flux functions, f and Q, and the initial data satisfy certain assumptions detailed below, then there is a finite breaktime T, such that the solution of the initial value problem (1.1), (1.2) satisfies

$$\lim_{t\uparrow T}\left\{\sup_x |u_x(x,t)|\right\} = \infty.$$

This theorem corroborates our intuitive understanding of the problem supported by the numerical results presented in [12]. Note that numerically we solve not the Cauchy problem, (1.1), (1.2), but rather the Dirichlet problem: equation (1.1) augmented with the initial-boundary value conditions,

$$\begin{aligned} &u(x,t=0) = u_0(x), && -L < x < L,\\ &u(\pm L,t) = u_0(\pm L), && t \geqslant 0. \end{aligned} \tag{1.3}$$

In section 2.2 we prove theorem 2.5, that extends the result obtained in theorem 2.1 to the initial-boundary value problem, (1.1), (1.3).

In section 2.3 we present several numerical examples. The use of a difference scheme based on the operator splitting method enables us to obtain a much better resolution of the subshocks, than was possible in [12]. We have also applied this scheme to the Cauchy problem to obtain qualitatively new numerical results for problem (1.1), (1.2) with large periodic initial data. We have observed a formation of subshocks for this problem as well. Though a complete proof of this fact is not available yet, our numerical studies make the behaviour of the solutions of equation (1.1) far more transparent—to the effect that for sufficiently large periodic initial data, the solution breaks down in a finite time. Moreover, we conjecture that given a nonconstant periodic function $\phi(x)$, then there exists a constant A such that the solution of (1.1), subject to the initial data

$$u(x,0) = A\phi(x),$$

breaks down in a finite time.

Section 3 is concerned with the proof of the breakdown when the dissipation flux is nonmonotone,

$$u_t + f(u)_x = \nu\left(\frac{u_x}{1+u_x^2}\right)_x, \qquad \nu > 0. \tag{1.4}$$

Note that if the initial datum is large enough (even if it is infinitely smooth), the questions of existence and uniqueness of solutions to the problem (1.4), (1.2) are highly nontrivial. Nevertheless, theorem 3.1 guarantees that its classical solution (if such a solution exists) will break down in a finite time.

In the second part of section 3 we develop a third-order central scheme based on the the nonoscillatory piecewise parabolic reconstruction (see [13, 14]). The use of this high-order scheme in conjunction with equation (1.4) allows us to improve the numerical results obtained in [11].

2. Equations with monotonic dissipation fluxes

We consider the model problem proposed in [12],

$$u_t + f(u)_x = Q(u_x)_x, \tag{2.1}$$

$$u(x,0) = u_0(x), \tag{2.2}$$

where the flux functions, f and Q, satisfy the following assumptions:

(i) $f(u)$ and $Q(s)$ are smooth functions of their arguments u and s, respectively;
(ii) f and Q have the symmetry properties needed to support odd solutions:

$$f(-u) = f(u) \qquad \forall u, \qquad Q(-s) = Q(s) \qquad \forall s;$$

(iii) f and Q are strictly monotone:

$$f'(u) > 0 \qquad \forall u > 0, \qquad Q'(s) > 0 \qquad \forall s;$$

(iv) f is unbounded, whereas Q is bounded, that is,

$$f(u) \to +\infty \qquad \text{as} \quad u \to +\infty, \qquad Q(s) \to Q_\infty < \infty \qquad \text{as} \quad s \to +\infty.$$

2.1. Initial value problem

In this section we prove breakdown of solutions of the initial value problem (2.1), (2.2) for the following class of initial data:

(a) u_0 is a smooth function;
(b) u_0 is skew symmetric, that is, $u_0(-x) = u_0(x) \qquad \forall x$;
(c) $\bar{u} \leqslant u_0(x) \leqslant 0 \qquad \forall x \geqslant 0$;
(d) $u_0(x) \leqslant \varphi(x) \qquad \forall x \geqslant 0$.

Here $\bar{u}$ is a large negative constant and $\varphi(x)$ is a profile to be determined.

Remark. Note that condition (d) means that the initial data, $u_0(x)$, are 'large enough'.

Theorem 2.1. *Consider the initial value problem (2.1), (2.2). Let hypotheses (i)–(iv) and (a)–(d) be satisfied. If u^* is a negative constant such that $f(u^*) > 2Q_\infty$, and if $\varphi(x)$ is a smooth function satisfying $\varphi(R) = u^*$ for some $R > 0$ and*

$$Q(\varphi_x)_x - f(\varphi)_x < 0 \qquad \forall x > 0; \tag{2.3}$$

then there exists T such that

$$\sup_x |u_x(x,t)| \to \infty \qquad \text{as} \quad t \uparrow T. \tag{2.4}$$

Before we turn to the proof of this theorem, we state and prove several auxiliary results.

Assertion 2.2. *Let hypotheses (i)–(iv) be satisfied. Then for any negative number $\bar{u}$ there is a (possibly large) $m > 1$ so that there is a viscous connection for a viscosity flux mQ. That is, there is a solution to the following boundary value problem,*

$$\begin{aligned} &f(\varphi)_x = mQ(\varphi_x)_x, \\ &\varphi(x) \to \pm\bar{u} \qquad \text{as} \quad x \to \pm\infty. \end{aligned} \tag{2.5}$$

Moreover, $\varphi(x)_{xx} > 0 \quad \forall x > 0$.

Proof. Note that due to the symmetry of the problem, $\varphi(x)$ has to be a skew symmetric function and therefore, problem (2.5) is equivalent to the following one:

$$\begin{aligned} &f(\varphi)_x = mQ(\varphi_x)_x, \qquad 0 < x < +\infty, \\ &\varphi(0) = 0, \qquad \varphi(x \to +\infty) = \bar{u}. \end{aligned} \tag{2.6}$$

Solving (2.6) we obtain

$$\int_0^{\varphi(x)} \frac{\mathrm{d}u}{Q^{-1}\left(\frac{f(u)-f(\bar{u})}{m}\right)} = x, \tag{2.7}$$

where Q^{-1} is an inverse function of Q, which exists due to the monotonicity assumption, (iii). Furthermore, the choice of sufficiently large m ensures that $\frac{f(u)-f(\bar{u})}{m}$ belongs to the domain of Q^{-1} for all $u \in [\bar{u}, 0]$, and this proves the existence of the desired profile $\varphi(x)$.

Next, it is easy to see that $\varphi(x) < 0$ and that $\varphi(x)$ is a monotone decreasing function. Consequently, $f(\varphi)_x > 0$, and we obtain that $\varphi_{xx} > 0$ due to the positivity of Q'. This completes the proof of assertion 2.2. □

Equipped with assertion 2.2 we now prove the following.

Proposition 2.3. *Let hypotheses (i)–(iv) be satisfied. Then, for any $u^* < 0$ there is a bounded skew symmetric function $\varphi(x)$ satisfying (2.3) and $\varphi(R) = u^*$ for some $R > 0$.*

Remark. Theorem 2.1 and proposition 2.3, together with the flux inequalities (iv) imply that there is a large class of smooth bounded initial data that leads to blow up of gradients in a finite time (see figure 1).

Proof. Let us take $\varphi(x)$ obtained in (2.7). Assertion 2.2 implies that

$$Q(\varphi_x)_x - f(\varphi)_x = (1-m)Q(\varphi_x)_x = (1-m)Q'(\varphi_x)\varphi_{xx} < 0 \qquad \forall x > 0,$$

since $m > 1$ and $Q' > 0$. Now take $\bar{u} = u^* - 1$. Since $\varphi(0) = 0$ and $\varphi(x) \to \bar{u}$ as $x \to +\infty$, we must have $\varphi(R) = u^*$ for some $R > 0$ due to the continuity of $\varphi(x)$. This proves the proposition. □

The purpose of proposition 2.3 and the assumptions (c) and (d) is to establish the following bounds on the solution of (2.1), (2.2):

Lemma 2.4. *Under the hypotheses (b)–(d) and inequality (2.3), a solution of the problem (2.1), (2.2) is bounded as follows:*

$$\bar{u} \leqslant u(x,t) \leqslant 0 \qquad \forall x > 0, \quad t < T \tag{2.8}$$

and

$$u(R,t) \leqslant u^* \qquad \forall t < T. \tag{2.9}$$

Proof. The solution $u(x,t)$ satisfies equation (2.1) for $x > 0$ and, due to the skew symmetry of $u_0(x)$, we also have $u(0,t) \equiv 0$. Therefore the bounds (2.8) are a consequence of comparison principles for scalar parabolic equations (see, e.g., [8]) and the initial bounds (c). Similarly, (d) and (2.3) imply

$$u(x,t) \leqslant \varphi(x) \qquad \forall t < T.$$

This yields (2.9) and the lemma follows. □

Equipped with lemma 2.4 we are now ready to complete the proof of theorem 2.1.

Proof of theorem 2.1. First, from the lower bound in (2.8) we obtain

$$\int_0^R u(x,t)\,\mathrm{d}x \geqslant R\bar{u}. \tag{2.10}$$

On the other hand, integrating equation (2.1) with respect to x over $(0, R)$ results with

$$\frac{\mathrm{d}}{\mathrm{d}t}\int_0^R u(x,t)\,\mathrm{d}x = -f(u(R,t)) + f(u(0,t)) + Q(u_x(R,t)) - Q(u_x(0,t)). \tag{2.11}$$

From the flux bound (iv), $|Q| \leqslant Q_\infty$, we obtain

$$|Q(u_x(R,t)) - Q(u_x(0,t))| \leqslant 2Q_\infty. \tag{2.12}$$

Also, as we have already mentioned, $u(0, t) = 0$, so

$$f(u(0, t)) = 0. \tag{2.13}$$

Finally, inequality (2.9) implies that

$$f(u(R, t)) \geqslant f(u^*) > 2Q_\infty. \tag{2.14}$$

Plugging (2.12)–(2.14) into (2.11) results with a positive constant α so that

$$\frac{\mathrm{d}}{\mathrm{d}t} \int_0^R u(x, t)\, \mathrm{d}x \leqslant -\alpha < 0.$$

This is inconsistent with the bound (2.10) and $\int_0^R u_0(x)\, \mathrm{d}x < 0$. This contradiction shows that the solution cannot remain regular beyond

$$T^* = -\frac{R\bar{u}}{\alpha}.$$

This concludes the proof of theorem 2.1. □

2.2. Dirichlet problem

We now turn to show an analogous breakdown for the Dirichlet problem. Let us consider equation (2.1) in the finite interval $-L < x < L$, subject to the initial-boundary conditions (1.3). Assumptions (i)–(iv), (a) and (b) are intact, while instead of (c) and (d) we assume:

(c′) $u_0(L) \leqslant u_0(x) \leqslant 0 \quad \forall x \in [0, L]$;
(d′) $u_0(x) \leqslant \varphi(x) \quad \forall x \in [0, L]$.

Note that due to its skew symmetry, problem (2.1), (1.3) is actually equivalent to the following initial-boundary value problem:

$$\begin{aligned} &u_t + f(u)_x = Q(u_x)_x, \qquad 0 < x < L, \\ &u(x, t = 0) = u_0(x), \qquad 0 < x < L, \\ &u(0, t) = 0, \qquad u(L, t) = u_0(L), \qquad t \geqslant 0. \end{aligned} \tag{2.15}$$

The result of theorem 2.1 can be extended to problem (2.15) as follows,

Theorem 2.5. *Consider the initial-boundary value problem (2.15). Let hypotheses (i)–(iv), (a), (b) and (c′), (d′) be satisfied. If u^* is a negative constant such that $f(u^*) > 2Q_\infty$, and if $\varphi(x)$ is a smooth function satisfying $\varphi(L) = u^*$ and*

$$Q(\varphi_x)_x - f(\varphi)_x < 0 \qquad \forall x \in (0, L); \tag{2.16}$$

then there exists T such that

$$\sup_{-L<x<L} |u_x(x, t)| \to \infty \qquad \text{as} \quad t \uparrow T.$$

We prove this theorem arguing along the lines of the proof of theorem 2.1. At first, we extend assertion 2.2 to the finite x-domain.

Assertion 2.6. *Let hypotheses (i)–(iv) be satisfied. Then, for any negative number u^*, there is an $m > 1$ such that there exists a solution to the following boundary value problem,*

$$\begin{aligned} &f(\varphi)_x = mQ(\varphi_x)_x, \\ &\varphi(0) = 0, \qquad \varphi(L) = u^*. \end{aligned} \tag{2.17}$$

Moreover, $\varphi(x)_{xx} > 0\ \forall x \in (0, L)$.

Proof. Solving (2.17) yields

$$\int_0^{\varphi(x)} \frac{\mathrm{d}u}{Q^{-1}\left(\frac{f(u)+c}{m}\right)} = x, \tag{2.18}$$

where the constants c and m are chosen so as to satisfy the second boundary condition, i.e.,

$$\int_0^{u^*} \frac{\mathrm{d}u}{Q^{-1}\left(\frac{f(u)+c}{m}\right)} = L.$$

Therefore, to prove the assertion we have to show the existence of c and m.

Note that by an appropriate choice of c, sufficiently large m, and due to the monotonicity of Q, $\varphi(x)$ defined by (2.18), can be bounded for all $x \in [0, +\infty)$. In this case we denote by $\bar{u} := \lim_{x\to+\infty} \varphi(x)$. Then $c = -f(\bar{u})$.

To complete the proof, we now define

$$G(\bar{u}, m) := \int_0^{u^*} \frac{\mathrm{d}u}{Q^{-1}\left(\frac{f(u)-f(\bar{u})}{m}\right)},$$

and show the existence of $\bar{u}$ and m such that

$$G(\bar{u}, m) = L. \tag{2.19}$$

It is easy to see that G is a continuous function in both arguments, and that

$$G(\bar{u}, m) > 0 \qquad \forall \bar{u}, m, \quad \text{and} \quad G(\bar{u}, m \to +\infty) \to +\infty. \tag{2.20}$$

On the other hand, setting $m = f(\bar{u})$, we obtain

$$\begin{aligned} G(\bar{u}, m = f(\bar{u})) &= \int_{u^*}^{0} \frac{\mathrm{d}u}{Q^{-1}\left(1 - \frac{f(u)}{f(\bar{u})}\right)} \\ &\leqslant |u^*| \cdot \max_{u\in[u^*,0]} \left\{ \frac{1}{Q^{-1}\left(1 - \frac{f(u)}{f(\bar{u})}\right)} \right\} = \frac{|u^*|}{Q^{-1}\left(1 - \frac{f(u^*)}{f(\bar{u})}\right)}. \end{aligned}$$

It is now clear that if we take sufficiently small $\bar{u} = \bar{u}_{min}$, then $Q^{-1}(1 - \frac{f(u)}{f(\bar{u})})$ will be greater than $2|u^*|$, and consequently,

$$G(\bar{u} = \bar{u}_{min}, m = f(\bar{u})) \leqslant \frac{L}{2}. \tag{2.21}$$

Finally, due to the continuity of G, it follows from (2.20) and (2.21) that there exist $\bar{u}$ and m which satisfy (2.19).

Moreover, we have shown that the solution of (2.17), $\varphi(x)$, also satisfies problem (2.5) with a corresponding value of $\bar{u}$. Hence, by assertion 2.2 we have $\varphi_{xx} > 0$, and the proof of assertion 2.6 is completed. □

All further steps of the proof of theorem 2.5 are identical to the proof of theorem 2.1 taking L instead of R. This implies a breakdown of the solution of the Dirichlet problem with a large initial-boundary conditions.

2.3. Numerical examples

We conclude section 2 with a number of new numerical results, which were obtained using the following second-order scheme based on the operator splitting approach (see, e.g., [7, 10, 1, 2, 5, 6, 9]).

Our splitting method can be summarized as follows. Let $S(t-\tau)$ be the exact solution operator associated with the corresponding conservation law,

$$v_t + f(v)_x = 0; \tag{2.22}$$

and let $H(s-\tau)$ be the exact solution operator associated with the corresponding nonlinear diffusion equation,

$$w_t = Q(w_x)_x. \tag{2.23}$$

This means that $v(x,t) = S(t-\tau)v(x,\tau)$ and $w(x,t) = H(t-\tau)w(x,\tau)$, respectively. Then we can construct the second-order splitting approximation in the following way:

$$u(x, t+\Delta t) \approx \left[S\left(\frac{\Delta t}{2}\right) \circ H(\Delta t) \circ S\left(\frac{\Delta t}{2}\right)\right] u(x,t). \tag{2.24}$$

To obtain a fully discrete splitting method one should use second-order accurate approximate solution operators, $\tilde{S}$ and $\tilde{H}$, instead of S and H, respectively. In the presented examples $\tilde{S}(\frac{\Delta t}{2})$ was obtained by means of the central Nessyahu–Tadmor scheme [16]. This scheme is BV-stable and converges to the unique entropy solution of (2.22) under the following CFL condition,

$$\Delta t \leqslant \frac{\Delta x}{\max\limits_u |f'(u)|}. \tag{2.25}$$

The approximate parabolic operator $\tilde{H}(\Delta t)$ was obtained by means of the standard central difference scheme,

$$w_j^{n+1} = w_j^n + \frac{\Delta t}{\Delta x}\left[Q\left(\frac{w_{j+1}^n - w_j^n}{\Delta x}\right) - Q\left(\frac{w_j^n - w_{j-1}^n}{\Delta x}\right)\right],$$

which is L^∞-stable under the different CFL condition, $\Delta t \leqslant \frac{(\Delta x)^2}{2\max_s Q'(s)}$.

In order to guarantee stability of the resulting scheme (for instance, in the strong L^∞-norm), we take Δt satisfying (2.25) and replace $\tilde{H}(\Delta t)$ by the composition of m operators, $\tilde{H}(\frac{\Delta t}{m}) \circ \tilde{H}(\frac{\Delta t}{m}) \circ \cdots \circ \tilde{H}(\frac{\Delta t}{m})$, where m is the minimal integer, such that

$$\frac{\Delta t}{m} \leqslant \frac{(\Delta x)^2}{2\max\limits_s Q'(s)}.$$

The resulting scheme can be written in the following operator form:

$$u(x, t+\Delta t) \approx \left[\tilde{S}\left(\frac{\Delta t}{2}\right) \circ \tilde{H}\left(\frac{\Delta t}{m}\right) \circ \cdots \circ \tilde{H}\left(\frac{\Delta t}{m}\right) \circ \tilde{S}\left(\frac{\Delta t}{2}\right)\right] u(x,t). \tag{2.26}$$

In figure 2 a numerical solution of the following problem,

$$u_t + (u^2)_x = \left(\frac{u_x}{\sqrt{1+u_x^2}}\right)_x, \tag{2.27}$$

augmented with the decreasing step-function initial data,

$$u_0(x) = \begin{cases} 1.2, & x < 0, \\ -1.2, & x > 0, \end{cases} \tag{2.28}$$

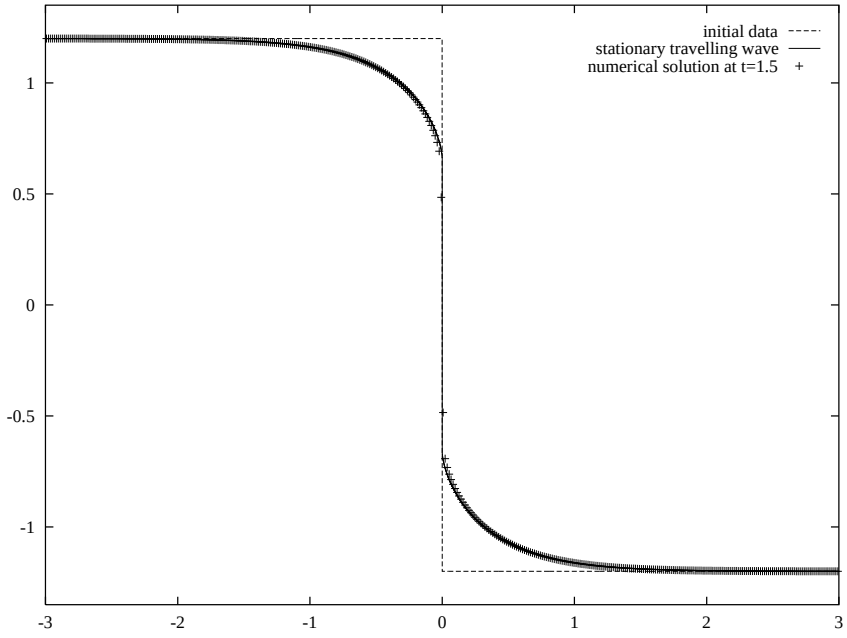

Figure 2. Riemann problem—(2.27), (2.28).

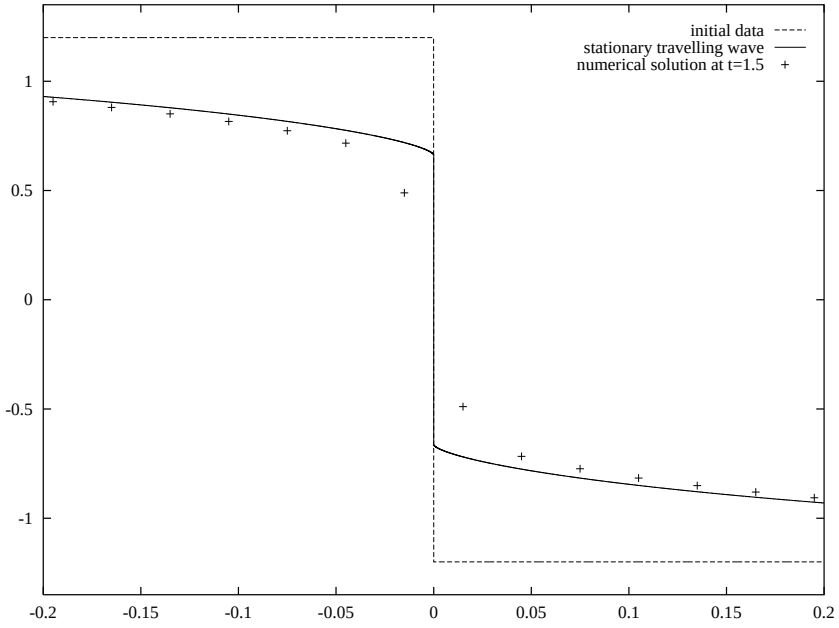

Figure 3. Problem (2.27), (2.28). $N = 200$; zoom on the $[-0.2, 0.2]$ interval.

is displayed (with the number of grid points $N = 400$). The numerical solution converges much better to the exact travelling wave solution than was possible to obtain by means of the nonsplitting, second-order Nessyahu–Tadmor-type scheme in [12]. To illustrate this

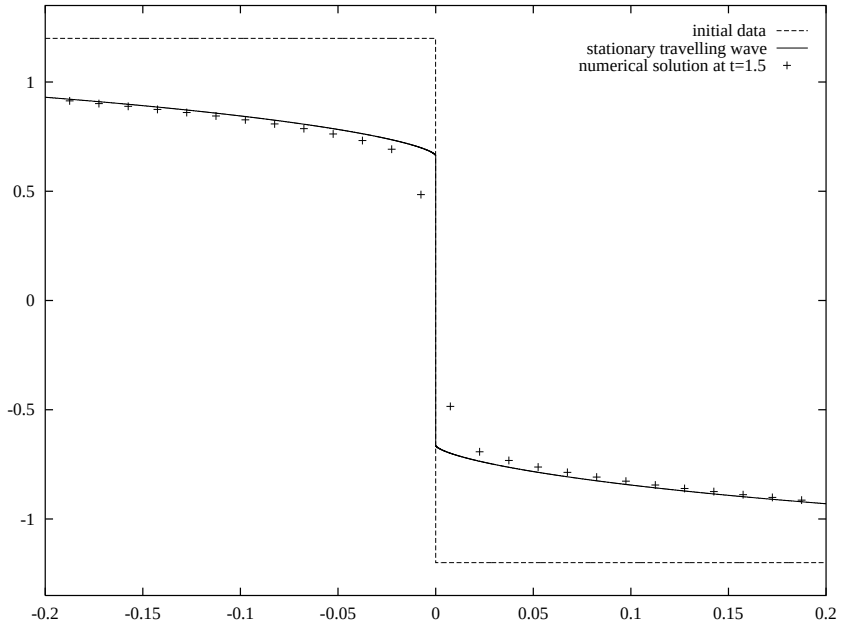

Figure 4. Problem (2.27), (2.28). $N = 400$; zoom on the $[-0.2, 0.2]$ interval.

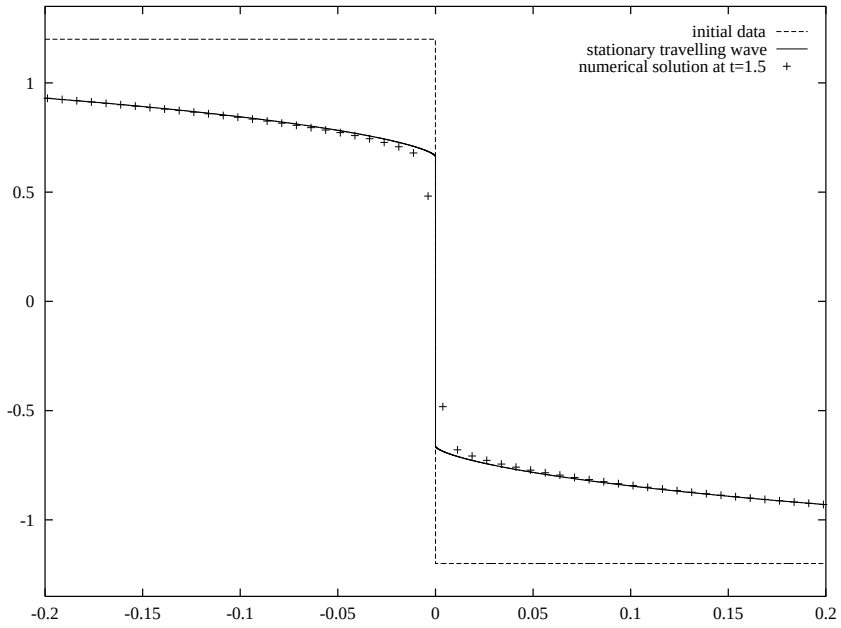

Figure 5. Problem (2.27), (2.28). $N = 800$; zoom on the $[-0.2, 0.2]$ interval.

convergence the numerical solutions with increasing number of grid points are shown in figures 3–6.

The same situation occurs when we compute the numerical solution to equation (2.27),

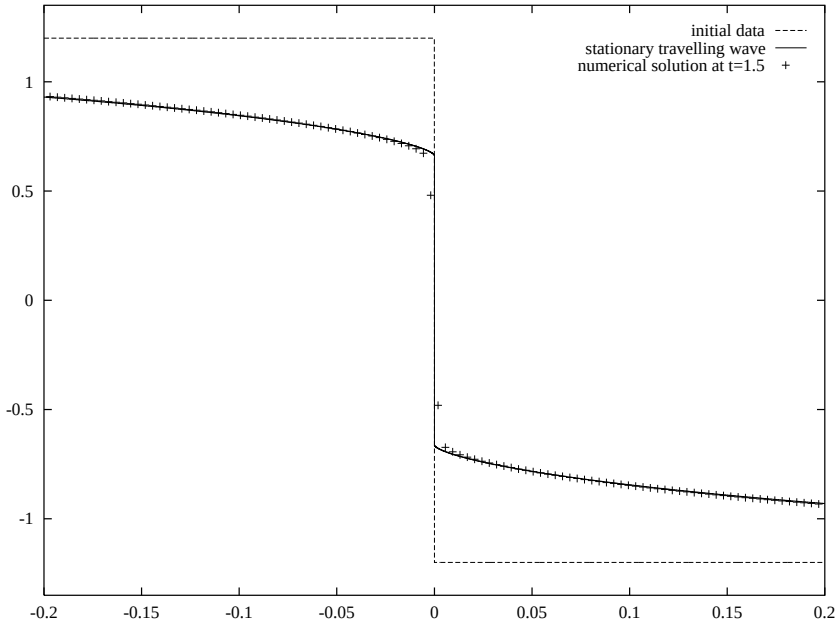

Figure 6. Problem (2.27), (2.28). $N = 1600$; zoom on the $[-0.2, 0.2]$ interval.

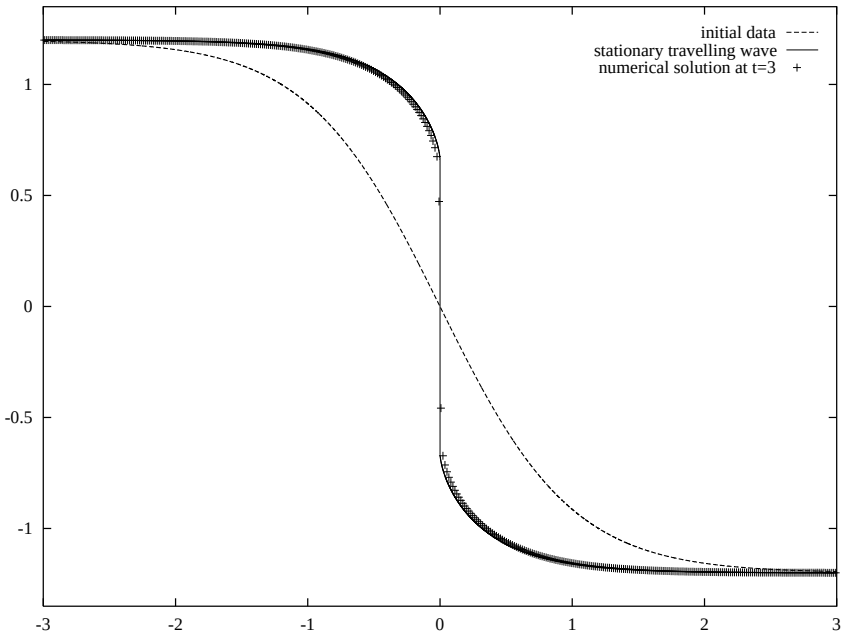

Figure 7. Tanh initial data for problem (2.27), (2.29).

subject to the following smooth initial data,

$$u_0(x) = -1.2\tanh(x). \tag{2.29}$$

The result for $N = 400$ is presented in figure 7.

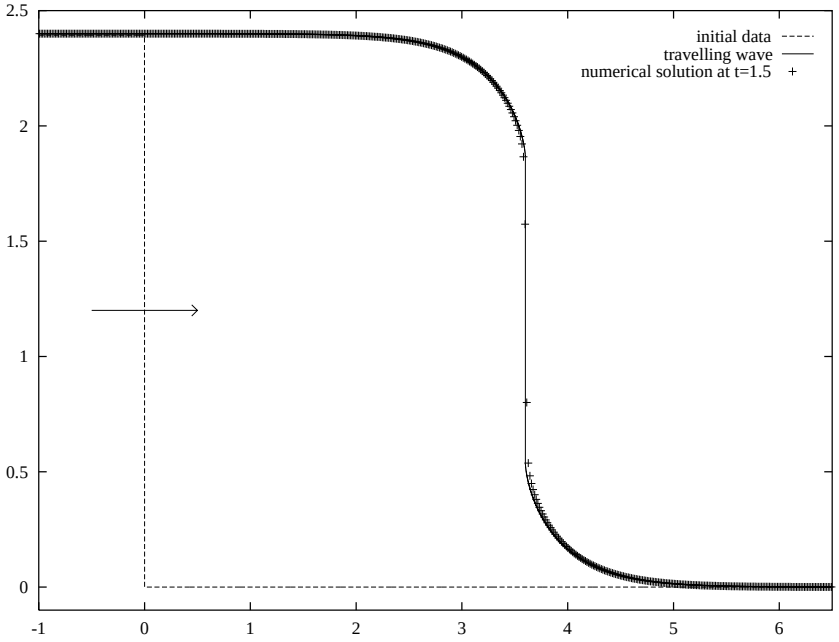

Figure 8. Asymmetric Riemann problem—(2.27), (2.30).

In both of these cases, a very good resolution of the discontinuity was obtained. Note that for the symmetric upstream–downstream values (± 1.2) used in these examples, the exact travelling wave solution is stationary.

Remark. In the second case of the smooth initial data, our numerical solution converges at a slower rate to its steady state: the solution to (2.27), (2.28) becomes stationary approximately at $t = 1.5$, and the solution to (2.27), (2.29)—at $t = 3$. Such a behaviour of the numerical solutions seems to us quite reasonable, although we lack a rigorous proof of this fact.

Finally, in figure 8 we display the 'moving' solution with asymmetric upstream-downstream values of 0 and -2.4, respectively: we solve numerically equation (2.27) augmented with the following initial data,

$$u_0(x) = \begin{cases} 2.4, & x < 0, \\ 0, & x > 0. \end{cases} \tag{2.30}$$

One can observe that in this case the resolution of the subshock is as good as in the stationary case.

In addition, we have used the same operator splitting method to solve numerically two Cauchy problems: equation (2.27) augmented with large periodic initial data—skew symmetric,

$$u_0(x) = 2\sin(x), \tag{2.31}$$

or asymmetric,

$$u_0(x) = \sin(x) + \cos(2x); \tag{2.32}$$

and small, periodic, initial data

$$u_0(x) = 0.5\sin(x). \tag{2.33}$$

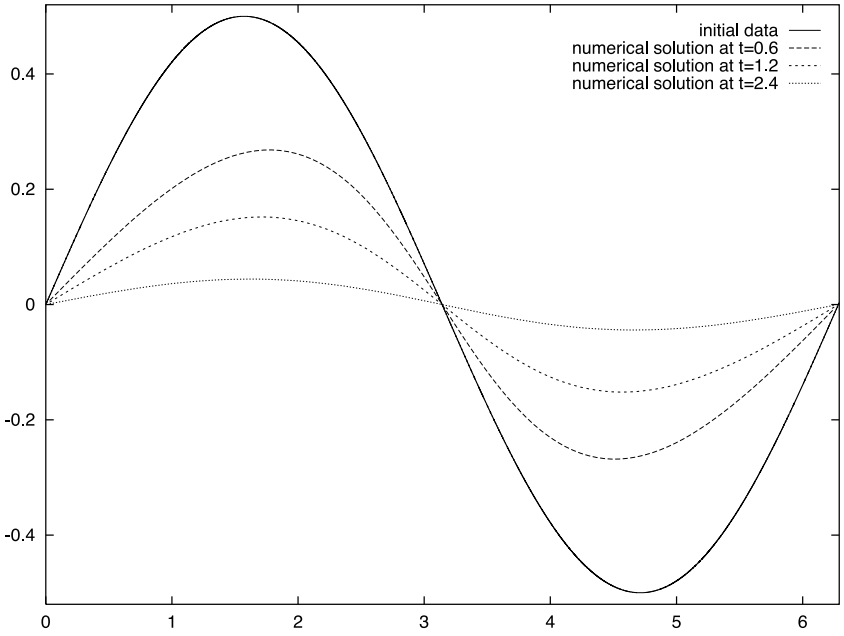

Figure 9. Small periodic initial data—problem (2.27), (2.33).

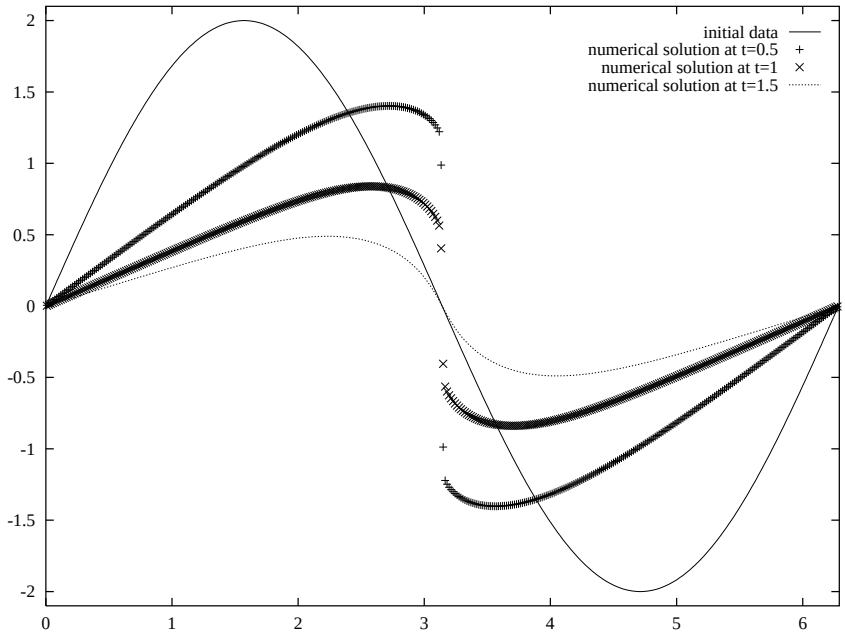

Figure 10. Large periodic initial data—problem (2.27), (2.31).

For the small initial data the resulting numerical solution of (2.27), (2.33) is plotted in figure 9. As was shown in [12, theorem 3.3], in this case the exact solution preserves its initial smoothness, and our numerical result confirms this fact. For the large initial data, like (2.31)

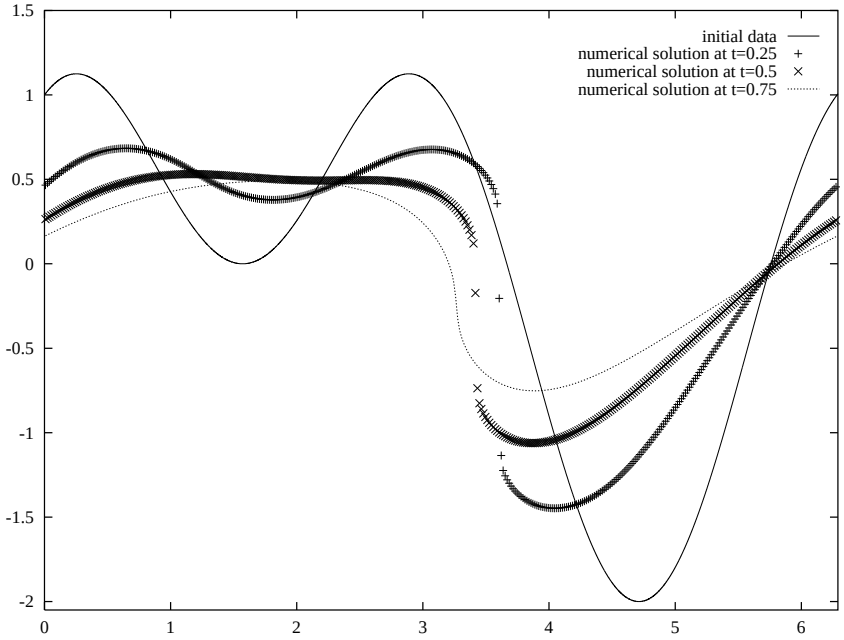

Figure 11. Large periodic initial data—problem (2.27), (2.32).

or (2.32), we were not able so far to prove what is clearly seen from the numerics in figures 10 and 11, namely; that large periodic initial data may induce a *formation of a discontinuity within a finite time*.

We would like to conclude section 2 by stressing that the breakdown results proved here are sharp in the sense that solutions will not break down if the dissipation flux is unbounded.

Lemma 2.7 (*a priori* estimate of u_x). *Consider equation (1.1) with a monotone Q such that $Q(s) \to \pm\infty$ as $s \to \pm\infty$. Then $u_x(x,t)$ is uniformly bounded for all $t > 0$.*

Proof. Let $U(x,t) \equiv \int^x u(x,t)$ denote the primitive of $u(x,t)$. Then it satisfies the following equation:

$$U_t + f(U_x) = Q(U_{xx}). \tag{2.34}$$

Differentiating (2.34) with respect to t we obtain a parabolic (due to the positivity of Q') equation in U_t,

$$(U_t)_t + f'(U_x)(U_t)_x = Q'(U_{xx})(U_t)_{xx}. \tag{2.35}$$

The maximum principle for (2.35) gives a uniform bound on U_t, while the maximum principle for the original equation (1.1) provides such a bound on $f(U_x)$. Therefore, from (2.34) we obtain that for all $t > 0$,

$$|Q(u_x)| \leqslant \text{const}.$$

Hence, $u_x(x,t)$ is uniformly bounded due to the monotonicity and the unboundedness of Q. □

3. Equation with a nonmonotone dissipation flux

In this section we consider the following model equation [11],

$$u_t + f(u)_x = Q(u_x)_x, \quad Q(u_x) = \nu \frac{u_x}{1+u_x^2}, \qquad \nu > 0. \tag{3.1}$$

The convection flux satisfies the following assumptions:

(I) $f(u)$ is a smooth function;
(II) $f(-u) = f(u)\ \forall u$;
(III) $f'(u) > 0\ \forall u > 0$;
(IV) $f(u) \to +\infty$ as $u \to +\infty$.

We study solutions of the initial value problem associated with (3.1) subject to initial data (2.2) which satisfy assumptions (a)–(d) in section 2.1. Our main concern in this section is the breakdown of the Cauchy problem.

3.1. Theory

Theorem 3.1. *Consider the initial value problem (3.1),(2.2). Let hypotheses (I)–(IV) and (a)–(d) be satisfied. If u^* is a negative constant such that $f(u^*) > \nu$, and if $\varphi(x)$ is a smooth function that for some $R > 0$ satisfies $\varphi(R) = u^*$, and*

$$Q(\varphi_x)_x - f(\varphi)_x < 0 \qquad \forall x > 0, \tag{3.2}$$

then there exists T such that

$$\sup_x |u_x(x,t)| \to \infty \qquad \text{as} \quad t \uparrow T.$$

Again, we proceed along the lines of the proof of theorem 2.1, and begin with the following assertion.

Assertion 3.2. *Let assumptions (I)–(IV) be satisfied. Then for any negative number $\bar{u}$ there exists an $m > 1$ (possibly a large one), such that there is a solution to the following boundary value problem,*

$$f(\varphi)_x = mQ(\varphi_x)_x, \qquad 0 < x < +\infty \tag{3.3}$$

$$\varphi(0) = 0, \qquad \varphi(x \to +\infty) = \bar{u}. \tag{3.4}$$

Moreover, $\forall x > 0$,

$$\varphi(x)_{xx} > 0 \qquad \text{and} \qquad -1 \leqslant \varphi(x)_x < 0. \tag{3.5}$$

Proof. Though $Q(s) = \nu \frac{s}{1+s^2}$ is in general nonmonotone, and hence noninvertible, on the interval $s \in [-1, 1]$, where its inverse, $Q^{-1}(z)$, exists and is defined via

$$Q^{-1}(z) = \frac{\nu - \sqrt{\nu^2 - 4z^2}}{2z}, \qquad |z| \leqslant \frac{\nu}{2},$$

it increases monotonously. Solving (3.3), (3.4) we obtain again,

$$\int_0^{\varphi(x)} \frac{\mathrm{d}u}{Q^{-1}\left(\frac{f(u)-f(\bar{u})}{m}\right)} = x. \tag{3.6}$$

Note that the integral in the LHS of (3.6) is defined for a sufficiently large m, since then $|\frac{f(u)-f(\bar{u})}{m}| < \nu/2$.

As before, $\varphi_x < 0$ and $\varphi_{xx} > 0$. Since

$$|\varphi_x| = \left| Q^{-1}\left(\frac{f(\varphi) - f(\bar{u})}{m}\right)\right| \leqslant 1,$$

it is also clear that $\varphi_x \geqslant -1$, and assertion 3.2 is thus proved. □

Next, by a complete analogy with the proof of proposition 2.3, we derive the following.

Proposition 3.3. *Let assumptions (I)–(IV) be satisfied. Then for any $u^* < 0$ and certain $R > 0$, there is a bounded skew symmetric function $\varphi(x)$ satisfying (3.2) and $\varphi(R) = u^*$.*

We now turn to the analogue of lemma 2.4.

Lemma 3.4. *Under the hypotheses (b)–(d) and inequality (3.2), a solution of the problem (3.1),(2.2) is bounded as follows:*

$$\bar{u} \leqslant u(x,t) \leqslant 0 \qquad \forall x > 0, \quad t < T \tag{3.7}$$

and

$$u(R,t) \leqslant u^* \qquad \forall t < T. \tag{3.8}$$

Proof. The bounds (3.7) are a simple consequence of the maximum principle for equation (3.1), which is valid. To prove the second bound, (3.8), we subtract (3.3) from (3.1) to obtain

$$(u-\varphi)_t + (f(u) - f(\varphi))_x = \nu\left(\frac{u_x}{1+u_x^2} - m\frac{\varphi_x}{1+\varphi_x^2}\right)_x. \tag{3.9}$$

Let $y(t) := \max_{x>0}(u(x,t) - \varphi(x)) = u(x_m(t),t) - \varphi(x_m(t))$. Note that *at the points of maximum*, $(x_m(t),t)$,

$$u_x = \varphi_x, \quad u_{xx} \leqslant \varphi_{xx}.$$

Thus, since $\nu > 0$, using the bounds (3.5), we conclude that the RHS of (3.9),

$$\nu\left(\frac{u_x}{1+u_x^2} - m\frac{\varphi_x}{1+\varphi_x^2}\right)_x = \nu\frac{1-\varphi_x^2}{(1+\varphi_x^2)^2}(u_{xx} - m\varphi_{xx}) \leqslant 0$$

at $(x_m(t),t)$. Consequently, we obtain the following ordinary differential inequality,

$$\dot{y}(t) + \varphi_x(x_m(t))f''(\xi)y(t) \leqslant 0, \tag{3.10}$$

where $\xi = \xi(t)$ is a midpoint between $u(x_m(t),t)$ and $\varphi(x_m(t))$. Integration of (3.10) yields the following inequality,

$$y(t) \leqslant y(0)\cdot\exp\left\{-\int^t \varphi_x(x_m(s))f''(\xi)\,\mathrm{d}s\right\},$$

which in turn implies the desired bound, (3.8), since by assumption (d), $y(0) \leqslant 0$. □

The last stage of the proof of theorem 3.1 is completely identical with the proof of theorem 2.1.

Remark. Our breakdown result, which was derived for the initial value problem (3.1),(2.2), can be also extended to the following Dirichlet problem,

$$\begin{aligned} &u_t + f(u)_x = \nu\left(\frac{u_x}{1+u_x^2}\right)_x, && -L < x < L,\\ &u(x,t=0) = u_0(x), && -L < x < L,\\ &u(\pm L,t) = u_0(\pm L), && t \geqslant 0. \end{aligned} \tag{3.11}$$

However, unlike the Dirichlet problem studied in section 2.2, in the present case L must be sufficiently large. Otherwise, there will be no solution of the corresponding boundary problem,

$$\begin{aligned} &f(\varphi)_x = \nu m\left(\frac{\varphi_x}{1+\varphi_x^2}\right)_x, \\ &\varphi(0) = 0, \quad \varphi(L) = u^*, \end{aligned} \tag{3.12}$$

for u^* satisfying $f(u^*) > \nu$. This is a possibility because, as was shown in assertion 3.2, $|\varphi_x| \leqslant 1$, and hence existence of the solution of (3.12) depends on the balance between L and u^*.

In other respects theorem 3.1 can be extended to problem (3.11) in the same way as theorem 2.1 was extended in section 2.2.

3.2. Numerical examples

In our previous works, [11, 12], the numerical solutions of equations (3.1) and (2.1) were computed using a second-order central Nessyahu–Tadmor-type scheme. Its stability was assured under an appropriate CFL condition. However, to satisfy this condition we had to take a very small time step, $\Delta t \sim (\Delta x)^2$, which caused the scheme to be overly dissipative and did not allow us to achieve a good resolution of discontinuities, [11, 12].

We note that the operator splitting method described in section 2.3 does not give any encouraging results when applied to equation (3.1): the numerical solution converges in time towards a piecewise constant stationary weak solution, which does not seem to be relevant. This happens since the nonmonotonicity of $Q(u_x)$ hampers the construction of a stable approximation of the diffusion operator, $H(t-\tau)$.

Our third-order scheme is based on a nonoscillatory piecewise parabolic reconstruction by Liu and Osher [13], $v(x,t^n) = \sum_j p_j(x)\chi_j(x)$, where each quadratic piece, $p_j(x)$, is of the form

$$p_j(x) = v_j^n + v_j'\left(\frac{x-x_j}{\Delta x}\right) + \frac{1}{2}v_j''\left(\frac{x-x_j}{\Delta x}\right)^2, \tag{3.13}$$

where v_j^n, $\frac{1}{\Delta x}v_j'$ and $\frac{1}{(\Delta x)^2}v_j''$ are approximate values of $u(x_j,t^n)$, $u_x(x_j,t^n)$ and $u_{xx}(x_j,t^n)$, respectively. Due to the conservation and accuracy requirements, these reconstructed pointvalues are uniquely given by

$$v_j' := \theta_j \frac{\bar v_{j+1}^n - \bar v_{j-1}^n}{2\Delta x}, \quad v_j'' := \theta_j \frac{\bar v_{j+1}^n - 2\bar v_j^n + \bar v_{j-1}^n}{(\Delta x)^2}, \quad v_j^n := \bar v_j^n - \frac{v_j''}{24}.$$

Here $\bar v_j^n$ denotes an approximate value of the average of $u(x,t^n)$ over the corresponding spatial cell $[x_{j-\frac12}, x_{j+\frac12})$ of uniform width $\Delta x \equiv x_{j+\frac12} - x_{j-\frac12}$; and θ_j is a nonlinear limiter, designed to prevent oscillations (consult [13, 14]).

This third-order accurate reconstruction, (3.13), is evolved in time using a central Nessyahu–Tadmor-type approach, that is, the staggered cell averages of $u(x,t^{n+1})$ are calculated via,

$$\begin{aligned} \bar v_{j+\frac12}^{n+1} = {}& \tfrac12[\bar v_j^n + \bar v_{j+1}^n] + \tfrac18[v_j' - v_{j+1}'] - \frac{1}{\Delta x}\left[\int_{\tau=t^n}^{t^{n+1}} f(v(x_{j+1},\tau))\,\mathrm{d}\tau - \int_{\tau=t^n}^{t^{n+1}} f(v(x_j,\tau))\,\mathrm{d}\tau\right] \\ &+ \frac{1}{\Delta x}\left[\int_{\tau=t^n}^{t^{n+1}} Q(v_x(x_{j+1},\tau))\,\mathrm{d}\tau - \int_{\tau=t^n}^{t^{n+1}} Q(v_x(x_j,\tau))\,\mathrm{d}\tau\right]. \end{aligned} \tag{3.14}$$

Next, we approximate the integrals in (3.14) by Simpson's quadrature rule, which is sufficient for retaining the overall third-order accuracy,

$$\frac{1}{\Delta x}\int_{\tau=t^n}^{t^{n+1}} f(v(x_j,\tau))\,\mathrm{d}\tau \sim \frac{\lambda}{6}[f(v(x_j,t^n)+4f(v(x_j,t^{n+\frac{1}{2}}))+f(v(x_j,t^{n+1})],$$

$$\frac{1}{\Delta x}\int_{\tau=t^n}^{t^{n+1}} Q(v_x(x_j,\tau))\,\mathrm{d}\tau \sim \frac{\lambda}{6}[Q(v_x(x_j,t^n)+4Q(v_x(x_j,t^{n+\frac{1}{2}}))+Q(v_x(x_j,t^{n+1})],$$

where $\lambda \equiv \frac{\Delta t}{\Delta x}$ is a constant ratio. The last two formulae, in turn, require the approximate pointvalues on the right, which can be computed via the Taylor expansion:

$$v(x_j,t^{n+\beta}) \approx v_j^n + (\beta\Delta t)v_t(x_j,t^n) + \frac{(\beta\Delta t)^2}{2}v_{tt}(x_j,t^n),$$

$$v_x(x_j,t^{n+\beta}) \approx \frac{1}{\Delta x}v_j' + (\beta\Delta t)v_{xt}(x_j,t^n) + \frac{(\beta\Delta t)^2}{2}v_{xtt}(x_j,t^n).$$

Here, the derivatives on the right are evaluated by exact differentiation of the quadratic reconstruction (3.13) and equation (3.1),

$$v_t(x_j,t^n) = -f'(v_j^n)\frac{v_j'}{\Delta x} + Q'\left(\frac{v_j'}{\Delta x}\right)\frac{v_j''}{(\Delta x)^2},$$

$$\begin{aligned} v_{tt}(x_j,t^n) = {} & [f'(v_j^n)]^2\frac{v_j''}{(\Delta x)^2} + 2f'(v_j^n)f''(v_j^n)\left(\frac{v_j'}{\Delta x}\right)^2 - 2f'(v_j^n)Q''\left(\frac{v_j'}{\Delta x}\right)\left(\frac{v_j''}{(\Delta x)^2}\right)^2 \\ & -4f''(v_j^n)Q'\left(\frac{v_j'}{\Delta x}\right)\frac{v_j'}{\Delta x}\cdot\frac{v_j''}{(\Delta x)^2} - f''(v_j^n)Q''\left(\frac{v_j'}{\Delta x}\right)\left(\frac{v_j'}{\Delta x}\right)^2\frac{v_j''}{(\Delta x)^2} \\ & -f'''(v_j^n)Q'\left(\frac{v_j'}{\Delta x}\right)\left(\frac{v_j'}{\Delta x}\right)^3 + Q'\left(\frac{v_j'}{\Delta x}\right)Q'''\left(\frac{v_j'}{\Delta x}\right)\left(\frac{v_j''}{(\Delta x)^2}\right)^3 \end{aligned}$$

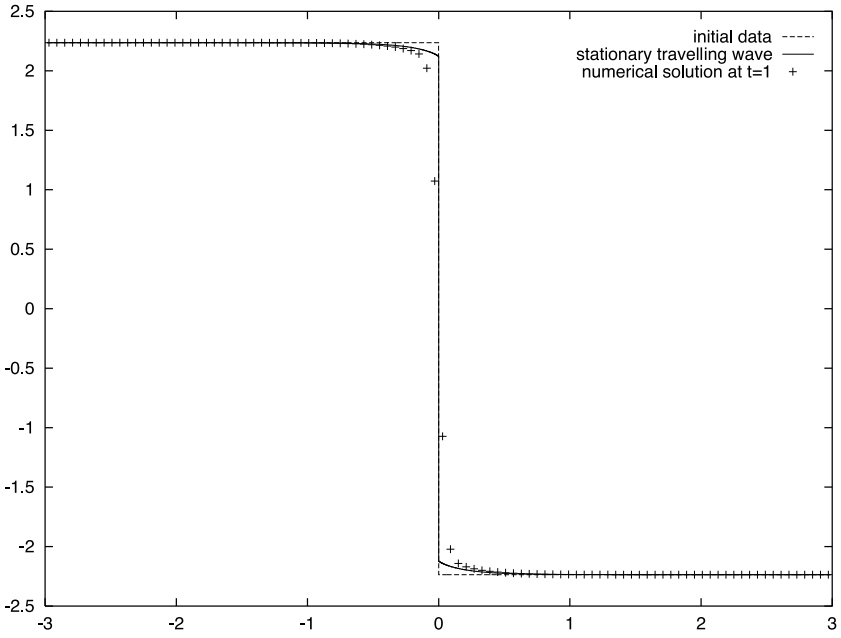

Figure 12. Initial value problem (3.15), (2.28). $N = 100$.

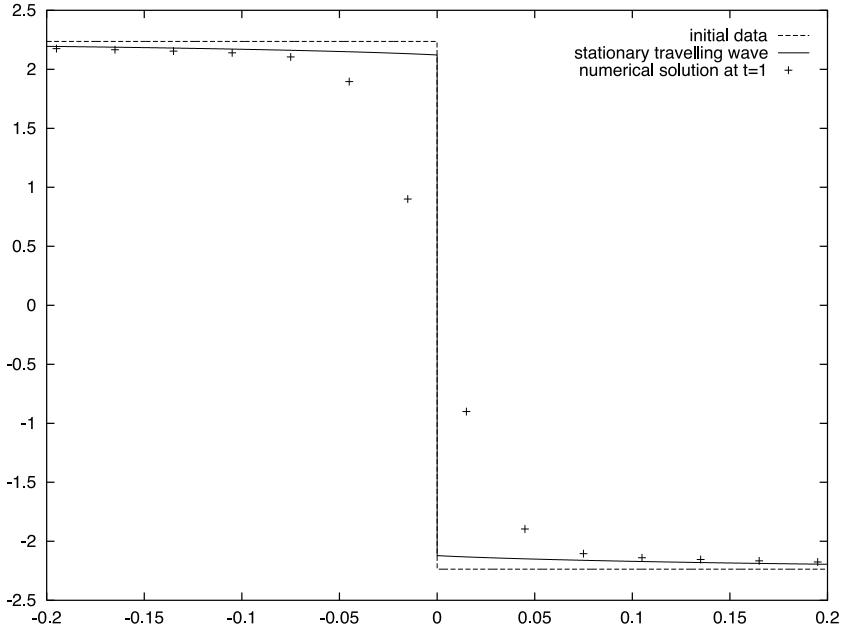

Figure 13. Problem (3.15), (2.28). $N = 200$; zoom on the $[-0.2, 0.2]$ interval.

$$+\left[Q''\left(\frac{v_j'}{\Delta x}\right)\right]^2\left(\frac{v_j''}{(\Delta x)^2}\right)^3;$$

$$v_{xt}(x_j,t^n) = -f'(v_j^n)\frac{v_j''}{(\Delta x)^2} - f''(v_j^n)\left(\frac{v_j'}{\Delta x}\right)^2 + Q''\left(\frac{v_j'}{\Delta x}\right)\left(\frac{v_j''}{(\Delta x)^2}\right)^2,$$

$$\begin{aligned} v_{xtt}(x_j,t^n) = {} & 6f'(v_j^n)f''(v_j^n)\frac{v_j'}{\Delta x}\cdot\frac{v_j''}{(\Delta x)^2} + 2f'(v_j^n)f'''(v_j^n)\left(\frac{v_j'}{\Delta x}\right)^3 + 2[f''(v_j^n)]^2\left(\frac{v_j'}{\Delta x}\right)^3 \\ & -2f'(v_j^n)Q'''\left(\frac{v_j'}{\Delta x}\right)\left(\frac{v_j''}{(\Delta x)^2}\right)^3 - f''(v_j^n)Q'\left(\frac{v_j'}{\Delta x}\right)\left(\frac{v_j''}{(\Delta x)^2}\right)^2 \\ & -8f''(v_j^n)Q''\left(\frac{v_j'}{\Delta x}\right)\frac{v_j'}{\Delta x}\left(\frac{v_j''}{(\Delta x)^2}\right)^2 - f''(v_j^n)Q'''\left(\frac{v_j'}{\Delta x}\right)\left(\frac{v_j'}{\Delta x}\right)^2\left(\frac{v_j''}{(\Delta x)^2}\right)^2 \\ & -f'''(v_j^n)Q'\left(\frac{v_j'}{\Delta x}\right)\left(\frac{v_j'}{\Delta x}\right)^2\frac{v_j''}{(\Delta x)^2} - f'''(v_j^n)Q''\left(\frac{v_j'}{\Delta x}\right)\left(\frac{v_j'}{\Delta x}\right)^3\frac{v_j''}{(\Delta x)^2} \\ & +Q''\left(\frac{v_j'}{\Delta x}\right)Q'''\left(\frac{v_j'}{\Delta x}\right)\left(\frac{v_j''}{(\Delta x)^2}\right)^4. \end{aligned}$$

By means of this third-order scheme we solve numerically the following initial value problem:

$$u_t + (u^2)_x = \left(\frac{u_x}{1+u_x^2}\right)_x, \tag{3.15}$$

subject to the decreasing step-function initial data, (2.28). The results obtained for different numbers of grid points, N, are displayed in figures 12–16.

Note that we still have to take $\Delta t \sim (\Delta x)^2$ to ensure the stability of our third-order

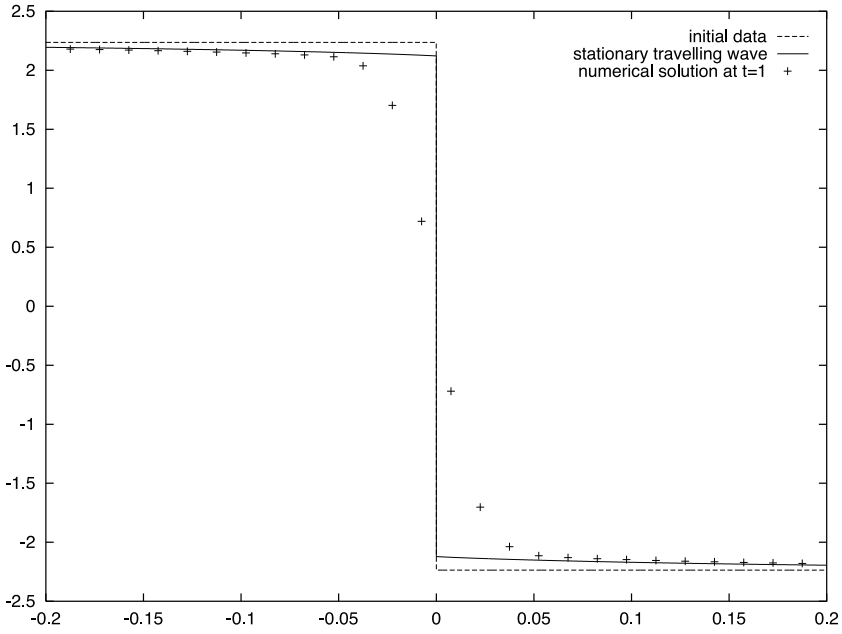

Figure 14. Problem (3.15), (2.28). $N = 400$; zoom on the $[-0.2, 0.2]$ interval.

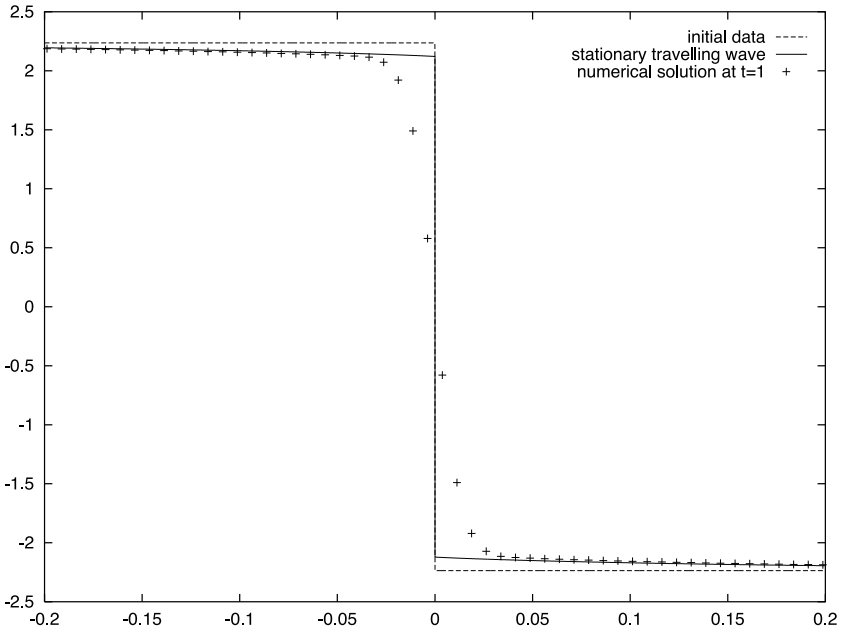

Figure 15. Problem (3.15), (2.28). $N = 800$; zoom on the $[-0.2, 0.2]$ interval.

scheme. Again, as in the case of the second-order scheme [11], a large amount of numerical dissipation can be observed. Therefore, in spite of its formal third order of accuracy, this scheme gives less satisfactory results than it was possible to obtain by the splitting method in

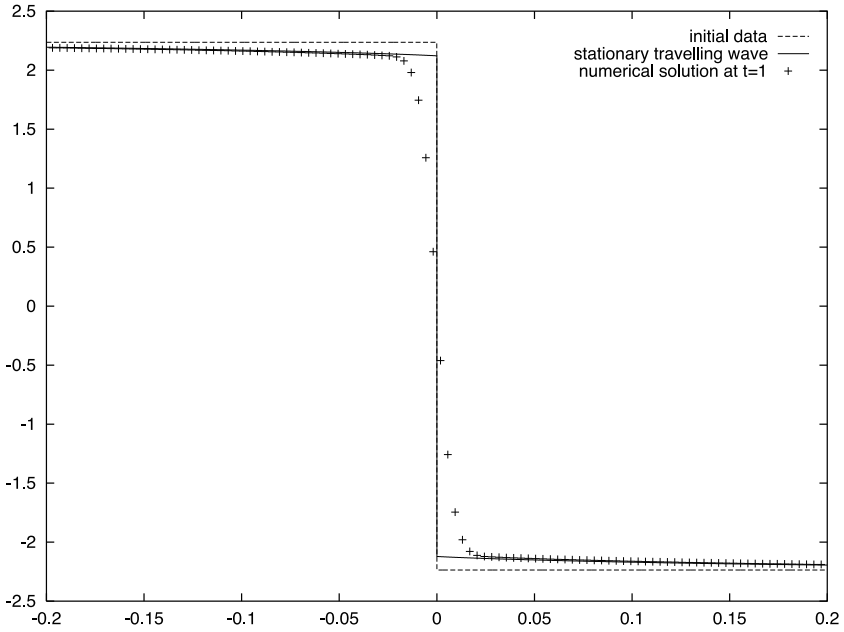

Figure 16. Problem (3.15), (2.28). $N = 1600$; zoom on the $[-0.2, 0.2]$ interval.

section 2.3. Nevertheless, the resolution of the subshock in figures 12–16 is much better than the one obtained in [11], and corroborates the analytical result of theorem 3.1.

Final remarks

(1) The numerical solution of the corresponding problem with the smooth initial data, (2.29), is quite similar and need not to be displayed.
(2) The breakdown of the solution of equation 3.1 with large periodic initial data was demonstrated numerically in [11].

Acknowledgments

The work of J Goodman was supported in part by the National Science Foundation and the Office of Naval Research. The work of P Rosenau was carried out, in part, during a stay at the Courant Institute of Mathematical Sciences, supported via the AFOSR Grant No. F49620-95-1-0065.

References

[1] Beale J T and Majda A 1981 Rates of convergence for viscous splitting of the Navier–Stokes equations *Math. Comp.* **37** 243–59
[2] Beale J T and Greengard C 1994 Convergence of Euler–Stokes splitting of the Navier–Stokes equations *Commun. Pure Appl. Math.* **47** 1083–115
[3] Bertsch M and Dal Passo R 1992 Hyperbolic phenomena in a strongly degenerate parabolic equation *Arch. Ration. Mech. Anal.* **117** 1–32
[4] Bertsch M and Dal Passo R 1992 A parabolic equation with a mean-curvature type operator *Nonlinear Diffusion Equations and Their Equilibrium States* vol 3, ed N G Lloyd *et al* (Boston, MA: Birkhauser) pp 89–97

[5] Dahle H K 1988 Adaptive characteristic operator splitting techniques for convection-dominated diffusion problems in one and two space dimensions *PhD Thesis* University of Bergen, Norway
[6] Dawson C N 1991 Godunov mixed methods for advective flow problems in one space dimension *SIAM J. Numer. Anal.* **28** 1282–309
[7] Evje S and Hvistendahl Karlsen K 1997 Viscous splitting approximation of mixed hyperbolic-parabolic convection-diffusion equations *Institut Mittag-Leffler Report (Stockholm, Sweden)*
[8] Friedman A 1964 *Partial Differential Equations of Parabolic Type* (Englewood Cliffs, NJ: Prentice-Hall)
[9] Hvistendahl Karlsen K and Ribero N H 1997 An operator splitting method for nonlinear convection-diffusion equations *Numer. Math.* **77** 365–82
[10] Hvistendahl Karlsen K and Ribero N H 1997 Corrected operator splitting for nonlinear parabolic equations *Applied Mathematics Report (University of Bergen, Norway)*
[11] Kurganov A, Levy D and Rosenau P 1998 On Burgers-type equations with non-monotonic dissipative fluxes *Commun. Pure Appl. Math.* **51** 443–73
[12] Kurganov A and Rosenau P 1997 Effects of a saturating dissipation in Burgers-type equations *Commun. Pure Appl. Math.* **50** 753–71
[13] Liu X-D and Osher S 1996 Nonoscillatory high order accurate self-similar maximum principle satisfying shock capturing schemes I *SINUM 33* **2** 760–79
[14] Liu X-D and Tadmor E 1996 Third order nonoscillatory central scheme for hyperbolic conservation laws *UCLA CAM Report* 96-42
[15] Malik J and Perona P 1990 Space-scale and edge detection using anisotropic diffusion *IEEE Trans. PAMI* **12** 629–39
[16] Nessyahu H and Tadmor E 1990 Non-oscillatory central differencing for hyperbolic conservation laws *J. Comput. Phys.* **87** 408–63
[17] Rosenau P 1990 Free energy functionals at the high gradient limit *Phys. Rev.* A **41** 2227–230
[18] Rosenau P, Hagan P, Northcutt R and Cohen D 1989 Delayed diffusion due to flux limitation *Phys. Lett.* A **142** 26–30